**Machine Vision & Applications manuscript No.**
(will be inserted by the editor)

# Fast Pattern Recognition using Normalized Grey-Scale Correlation in a Pyramid Image Representation

**W. James MacLean**[1]**, John K. Tsotsos**[2]

[1] University of Toronto, Department of Electrical & Computer Engineering, Toronto, Canada M5S 1A1

[2] York University, Department of Computer Science, Toronto, Canada M3J 1P3

February 16, 2007

**Abstract** The ability to quickly locate one or more instances of a model in a grey scale image is of importance to industry. The recognition/ localization must be fast and accurate. In this paper we present an algorithm which incorporates normalized correlation into a pyramid image representation structure to perform fast recognition and localization. The algorithm employs an estimate of the gradient of the correlation surface to perform a steepest descent search. Test results are given detailing search time by target size, effect of rotation and scale changes on performance, and accuracy of the subpixel localization algorithm used in the algorithm. Finally, results are given for searches on real images with perspective distortion and the addition of Gaussian noise.

*Send offprint requests to*: W. James MacLean

## 1 Introduction

Fast pattern recognition is an invaluable component of many machine-vision algorithms used in industry today. The ability to quickly identify an object, or a marking on an object can aid in finding a desired part among a group of parts, or to register a part so that work may be performed on it. This paper outlines an algorithm for fast detection and localization of a pattern using simple and inexpensive hardware. For example, typical search times are less than 0.25 S, and as low as 10–30 mS when the expected number of targets is known in advance.[1] Specifically, the algorithm is suitable for implementation on a personal computer equipped with an image acquisition board and a camera.

The algorithm relies on a pyramid representation of both the model image and the search image, as well as an estimate of the gradient of the correlation surface. The algorithm begins by creating a pyramid representation of the model image. A worst-case analysis is then used to determine the effect on the correlation score of i) the number of pyramid levels combined with ii) the possible different registrations of the pyramid sampling grid with respect to the model, in order to determine the optimum number of pyramid levels to use. This analysis is done once off-line.

During the search phase, a pyramid representation is built from the image being searched for instances of the model. It is built to the same depth as the model pyramid. The top-level of the model pyramid is convolved with the top-level of the search-image pyramid to produce a correlation surface from which likely can-

[1] These times are reported for a 750 MHz Athlon processor.

didates for model instances can be chosen. For each candidate, the search process descends through the pyramid performing a steepest descent search based on the correlation-gradient at each level. When the bottom level is reached, either a model instance has been found or the candidate is rejected for failing to meet a minimum threshold for its correlation score. Once a model instance is found, a bi-quadratic sub-pixel localization algorithm can be applied if desired. Figure 1 shows an overview of the search algorithm.

Correlation does not generally allow for size or rotational orientation variations, nor does it allow for model instances which are partially occluded. Non-uniform lighting variations will also detract from the algorithm's performance, but it is assumed that these may be controlled in industrial settings. Despite these drawbacks inherent in correlation-based matching, our algorithm is suitable for incorporation into larger algorithms that address the issues of size and rotation variance, possibly through the use of multiple search templates giving information about a target in different sizes and orientations. It is also suitable for extending matching methods based on principal components analysis (PCA), such as those found in [37,26].

An outline of this paper is as follows: results of previous approaches are considered in section 2. Section 3 deals with the idea of performing normalized grey-scale correlation in a pyramid structure. Section 3.1 develops an estimate of the correlation gradient for gradient-descent search. An important feature of this estimate is that it can be computed quickly. In section 3.3 a method for choosing the depth of the pyramid is presented. Section 4 describes details of the algorithm's implementation and gives performance results. A discussion of the results of applying the algorithm are presented in section 5.

## 2 Review of Previous Work

The problem of finding targets in images involves two important steps: *localization* of candidate matches within the image, and verification of each candidate through a *matching* process. Most of the relevant literature in the field involves the task of matching, and as such assumes that the images being compared are of the same size. Matching algorithms can be broken down into two major categories, those based on correlation and those based on features. The latter category includes features based on colour, gradient orientation, moments and shape descriptors. Matching algorithms often ignore issues related to scale and orientation, leaving those to be determined during the localization stage. The task of localization involves finding the right region within the search image (including determining the region's size) and passing this region to the verification process.

Some of the earliest attempts at matching have been done using correlation methods, which are reviewed in detail in [10, 29, 5]. The concept of normalized correlation was developed to combat the effect of different illumination levels on these techniques. A major downfall of correlation techniques is that, when combined with naive localization methods such as brute-force search, they are computationally very intensive, and as such tend to be slow. Despite this, they have remained popular with the advent of appearance-based matching methods such as eigenfaces and related techniques [37, 26]. Another class of techniques involves matching moments [29], but is limited to the case where localization has already been performed, and the pattern to be matched has been segmented from the background prior to applying the moment operators. When this can be done these techniques are often powerful, as they can provide rotation and size invariant recognition [11, 6], although the issue of localization is seldom addressed. Other moment-based approaches include [13, 41, 15], with the latter using Zernicke moments computed using polar coordinates.

Combining an approach similar to correlation with feature-type matching, both [27, 13] use deformable templates to match models to target instances. In [13] the matching is performed on candidates retrieved using feature vector indexing. The amount of warp and discrepancy in the resulting edge maps is used as a measure of similarity to rank the top matches. Matches are performed on binary images. Nastar *et. al.* [27] performs image matching using pixel intensities in a method described as a generalization of optic flow and eigenfaces. Also based on deformable templates, a description is given in [31] of a search technique which is somewhat robust to scale changes and moderate rotation about the vertical axis. The technique involves dividing the target into columns, and allowing pixels from each column to match one or more columns in the search image using a dynamic programming method. Robustness to moderate scale change is provided by searching over three pre-defined scales in the search image. While it is claimed that this technique is superior to NGC (normalized grey-scale correlation), no timing comparison is done.

There exist a number of techniques for matching entire images [28,33,13,41]. These techniques typically generate indices to allow fast retrieval of similar images from a database, and they often assume that images have been normalized in size. In [28] appearance-based matching is used to index into a database of images. This work is largely based on eigen-image matching with a Karhunen-Loeve transformation to limit the size of the basis space required. In a method similar to work reported later in [27], shape matching based on eigenmodes is also used to index into the database.

One class of approaches to matching is based on extracting features from the images under consideration. Two popular features are colour [4,33,41] and edge orientation [33,18,13]. Colour features usually involve matching colour histograms over the region of interest, but they are only applicable to colour images. In [33] a technique for indexing images based on both colour and edge-orientation histograms is given, with the intent of matching via nearest neighbour techniques. Similarly [13] uses colour histograms with moment invariants as an indexing feature to find top candidates for subsequent matching with deformable templates. In [4] the authors present a colour histogram matching metric, and demonstrate its usefulness by finding Waldo in images from the popular "Where's Waldo?" series. Since the histograms are computed over local regions of fixed size, the technique is not only able to detect Waldo but also find his location. In [41] colour histograms are combined with Fourier, moment-invariants and intensity projection onto $x$ and $y$ axes to provide a means for indexing into a trademark database. Both [33,13] use edge orientation histograms to provide indexing for matching. In a different vein, Lowe [18, 19] computes local features based on magnitude and orientation information at image regions determined to have stable responses to a difference-of-Gaussians filter, across multiple scales. The novel aspect of this work is that it matches features in the target to features in a search image based on a Hough transform for accumulating pose parameters. This estimation of pose parameters seeks to solve localization as well as matching. This method is better described as a parts-based object recognition scheme, even though no semantics are attached to individual features. The performance is fast (estimated to be on the order of 100 mS or better on modern hardware), and is tolerant to scaling and rotation in, and to some extent out, of the image plane. The features used are, however, sensitive to global changes in illumination [3], unlike normalized correlation. Lowe's technique is not expected to be easily applied to small targets, for example an $8 \times 8$ target, as it will be difficult to assess stability across scales since details will disappear quickly as coarser scales are attempted. Further, this method does not appear to be suitable for sub-pixel localization of the target. A number of affine-invariant feature detection techniques have been developed in recent years [1, 21–23, 25, 24]. Maximally-stable extremal regions (MSER) [1] is a technique that identifies regions based on their stability when thresholded using a range of thresholds. These stable regions are considered features, and suitable descriptors can be used to describe their content. A number of affine-invariant descriptors [21–23] are based on applying the standard Harris-Stephens corner detector [9] across multiple scales to find a maximal response, and computing an elliptical region around the feature location whose scale and orientation can be used to created an affine-invariant descriptor for the feature. These descriptors, like SIFT descriptors, are useful for comparing features across different images and across different scales and orientations. These techniques have proven useful in content-based image retrieval and indexing in video sequences [35], using the “bag of features” concept. Any of the techniques involving image gradients may run into problems for artificial images with high contrast and considerable regularity in edge orientations, for example corporate logos.

Another feature approach involves the use of probabilistic features [32, 36]. In [32] object appearance is encoded using estimates of joint density functions for the recovered features. While this system is fast (on the order of 100 mS on an SGI O2 workstation), it is only intended for detection and not localization (localization accuracy is 30 to 80 pixels). Stauffer & Grimson [36] use a set of training images of the target to learn a joint distribution of pixel intensities in an image patch. Comparison of the joint density to that of a candidate image patch takes about 1 second on a 500 MHz pentium, making the method too slow for fast object localization.

A new class of technique is centred around neural networks, but to date they are more suited to pattern classification than localization. Kulkarni [16] describes a size/rotation invariant object recognition method using back propagation to recognize feature vectors, but the vectors are based on moments and thus are good for matching but not localization. Work done by Wechsler & Zimmerman [39, 40] looks more promising, but seems too complex to be fast on modest hardware. In [12] neural networks are used to learn optimal templates for nearest neighbour matching. In [41] a neural network is used to classify based on recovered feature vectors.

Finally, the concept of using pyramid representations for image analysis is certainly not new, and is closely linked to the theory of scale-space [14, 17]. In this paper pyramid representations are used to overcome some of the computational problems associated with correlation methods. Burt [2] has constructed a pyramid-based attention model which uses Gaussian and Laplacian pyramids, and which is used for foveation, tracking and determining where to look next based on image saliency. Their system can be used for pattern recognition by using a pattern tree to represent salient features of objects at different resolutions. If enough features are matched, then the pattern has been found. Special hardware has been developed [38] to aid in the construction of image pyramids. Lowe [18] uses multiple image scales to determine the stability of features. Ramapriyan *et al.* [30] uses a multi-level decision tree approach to finding templates in images. A set of target templates is partitioned in a manner that allows subsets of templates to be removed from consideration should initial computations at a particular image location contraindicates. If evidence supports further search, the candidates under consideration is narrowed until a best match occurs. Since only a small number of matches are expected over the large number of possible image locations, search speed is greatly improved. In [7] Greenspan proposes a decision tree method for determining 3-D object pose in images, again making use of hierarchical search in pattern matching.

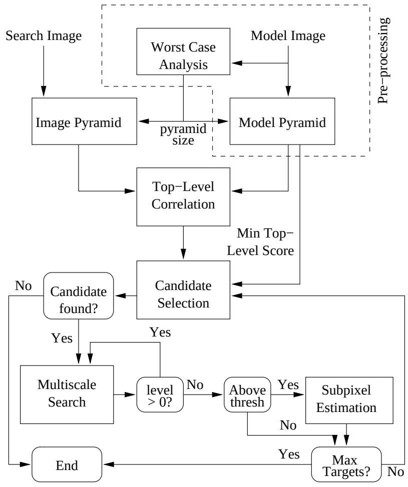


**Fig. 1** Overview of pyramid-based NGC search.

## 3 NGC in a Pyramid Representation

This section describes the use of a pyramid image representation to reduce the computational complexity associated with correlation search. Let $I(x, y)$ represent an image $I_w \times I_h$ pixels in size. The top-left corner of the image is defined to be the origin. Each pixel is assumed to encode a grey value in the range $0 \ldots 255$, one byte per pixel, although colour correlation is easily achieved by replacing pixel multiplications with inner-product operations performed on RGB values represented as vectors. If we wish to use correlation to search for a model $M(x, y)$ of size $M_w \times M_h$ in the image, the complexity for performing the correlation is $\mathcal{O}(I_w I_h M_w M_h)$. However, the cost of the computation increases considerably if normalized correlation is used (see Eq. 1).

$$C(x,y) = \frac{G(M(0,0), I(x,y))}{\sqrt{G(M(0,0), M(0,0))G(I(x,y), I(x,y))}} , \qquad (1)$$

where

$$G(f_1(x_1,y_1),f_2(x_2,y_2)) = \sum_{i=0}^{M_w-1}\sum_{j=0}^{M_h-1} f_1(x_1+i,y_1+j)f_2(x_2+i,y_2+j)$$

and $x < I_w - M_w + 1$ and $y < I_h - M_h + 1$.

An overview of the method is as follows: build pyramid representations of both the model and the image (search space), and perform correlation search at the top levels of the two pyramids. This can be done very quickly due to the reduced image sizes. The best match at the top level can be refined using a coarse-to-fine strategy in which the best estimate of location at level $k$ in the pyramid is used as the starting point for the search at level $k-1$. When the base of the pyramid is reached, the model has been found. Multiple instances can be found through repeating this procedure by choosing more than one match at the top level of the pyramid.

We now describe briefly the method of building both the image pyramid and the model pyramid. The structure of the pyramid is quite simple. We have used an averaging-with-no-overlap scheme, and use a sub-sampling rate of 2. This means that each level in the pyramid has dimensions equal to one-half of those for the level below, meaning that each level is one-quarter the size of the one immediately below. Each pixel in a given layer is the average of four pixels from the layer below. These four pixels are termed the receptive field of the pixel on the higher level, and the fact that the pyramid is non-overlapped means that on each level the receptive fields do not overlap each other. This type of pyramid can be built quickly, as each pixel in a new level only requires 3 adds and one shift to compute. The algorithm for building the pyramid is $\mathcal{O}(I_w I_h)$. The number of levels is limited

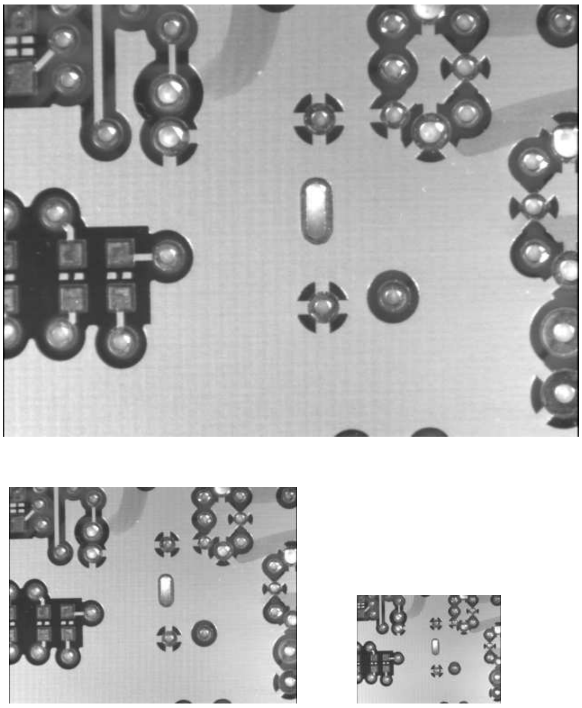

**Fig. 2** The pyramid representation for a typical image is shown. The pyramid has three levels, with level 0 being the largest image at $320 \times 240$ (top), and level 2 being the smallest at $80 \times 60$ (bottom right). In the level 0 image, a search model is defined.

by $K_{max} \leq \log_2 min(M_w, M_h)$. The advantages of building a pyramid become quickly obvious: the $K$th-level of a pyramid has $2^{2(K-1)}$ times fewer pixels than does the original image. Remember that the model pyramid at level K also has $2^{2(K-1)}$ times fewer pixels than at its level 0, so that the total cost of NGC at the top level of the pyramid is $2^{4(K-1)}$ times smaller than NGC on the original image. For a 4-level pyramid, this factor is 4096.

To perform correlation search for the model at the top-level of the pyramid, the complexity is $\mathcal{O}((I_w I_h M_w M_h)/2^{4(K-1)})$. Of course, the localization of the

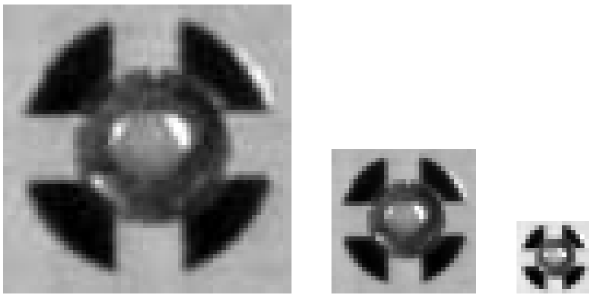

**Fig. 3** The pyramid representation of the model in Figure 2 is shown. It has the same number of levels as the image pyramid.

pattern at the top level of the pyramid is not perfect, but this can be used as an initial estimate for the next level of the pyramid. At each level of the pyramid a small number of correlations is used to refine the location estimate.

Instead of performing an exhaustive local search for the new maximum at each level of the pyramid, it is possible to estimate the gradient of the correlation surface and use a steepest descent method to perform the search. The following section describes the derivation of the gradient estimate.

### *3.1 Derivation of Correlation Gradient*

When the estimate of model location is refined at each level of the pyramid, it is possible to use an estimate of the gradient of the correlation surface to perform a steepest descent search. While it is possible to estimate the correlation surface in a $3 \times 3$ neighbourhood centred on the current location estimate, this is computationally expensive (it requires 9 full correlations). It is possible to estimate the correlation gradient in a less expensive manner. However, in applying steepest descent to a surface that we expect will have multiple maxima, it is important to identify regions expected to contain local maxima to allow the search to converge quickly. The use of the image pyramid does this: not only does it limit complexity of the top-level correlation, but it facilitates finding candidate regions and provides a means of quickly refining the search. In the derivation which follows the continuous case is developed: the transition to the discrete case is straighforward.

Given an image $I(x, y)$ and a model $M(x, y)$, with $M$ being differentiable over all $x$ and $y$, the correlation coefficient surface can be defined as

$$C(u, v) = \frac{\int_{\infty}^{\infty}\int_{\infty}^{\infty} I(x, y)(MW)(x - u, y - v)dx\, dy}{\left[\int_{\infty}^{\infty}\int_{\infty}^{\infty} I^2(x, y)W(x - u, y - v)dx\, dy\right]^{1/2}} \; . \tag{2}$$

(Note: the integration limits in subsequent equations are the same, but are omitted for compactness of notation.) The function $W(x, y)$ is a windowing function which is used to force the contribution from $M$ to zero at its boundaries:

$$W(x, y) = 0 \; \forall \; x < 0, \; x > M_w, \; y < 0 \text{ and } y > M_h \; . \tag{3}$$

The notation $(MW)(x, y)$ is shorthand for $M(x, y)W(x, y)$. For simple correlation computation, $W$ is normally chosen to be a box function. However, since we will want to differentiate Eq. 2, the windowing function should be chosen such that its derivative goes to zero at the borders of the window. It is assumed that $\int\int M^2(x, y)W(x, y)dx\, dy = 1$, *i.e.* that $M(x, y)$ is normalized with respect to the windowing function. Since this need only be done once, it can be done offline before the search is performed. Assuming that our functions $M$ and $W$ are well-behaved we can differentiate Eq. 2 to derive the gradient:

$$\nabla C(u, v) = \begin{bmatrix} \frac{\partial C}{\partial u} \\ \\ \frac{\partial C}{\partial v} \end{bmatrix} \; . \tag{4}$$

The gradient of the windowed correlation is

$$
\begin{aligned}
\nabla C^2(u,v) = \quad & -2\frac{\iint I(x,y)(MW)(x-u,y-v)dx\,dy}{\iint I^2(x,y)W(x-u,y-v)dx\,dy} \\
& \times \iint I(x,y)\nabla(MW)(x-u,y-v)dx\,dy \\
& + \quad \left[\frac{\iint I(x,y)(MW)(x-u,y-v)dx\,dy}{\iint I^2(x,y)W(x-u,y-v)dx\,dy}\right]^2 \\
& \times \quad \iint I^2(x,y)\nabla W(x-u,y-v)dx\,dy \ .
\end{aligned}
$$

This leaves us with just four terms to calculate:

$$\iint I(x,y)(MW)(x-u,y-v)dx\,dy \tag{5}$$

$$\iint I(x,y)\nabla(MW)(x-u,y-v)dx\,dy \tag{6}$$

$$\iint I^2(x,y)W(x-u,y-v)dx\,dy \tag{7}$$

$$\iint I^2(x,y)\nabla W(x-u,y-v)dx\,dy \tag{8}$$

Since $C^2(u,v) \in [0,1]$ we don't expect $\nabla C^2(u,v)$ to be huge so long as the correlation surface is reasonably smooth, *i.e.* no discontinuities in $I$ or $M$. As the amount of high-frequency content in $M$ and/or $I$ increases, we expect the correlation surface to become less smooth. When we move to the discrete case, the derivative becomes a difference and hence will always exist, but it is still desirable to avoid large discontinuities in the model and image. Fortunately, the pyramid-building operation also acts as a low-pass filter, making gradient magnitudes manageable.

### *3.2 Choice of Image Vector Space Origin*

Modern imaging technology typically represents images as one (or more) 2-D arrays of 1-byte pixels, with individual pixels having values in the range of $0 \ldots 255$.

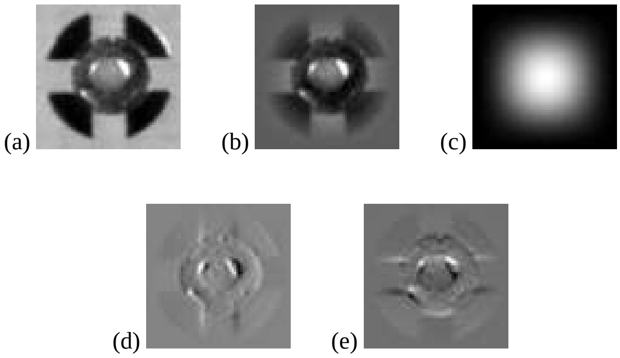


**Fig. 4** This figure shows the various representations required at each level of the pyramid for gradient correlation search. The model is given in (a). The windowed version of the model is shown in (b), with the windowing function shown in (c). The horizontal and vertical components of the gradient are shown in (d) and (e).

While correlation values are in the range of $-1$ to $1$, images represented solely by non-negative integers will lead to purely non-negative correlation values.

An important example of this occurs when comparing the model to a section of the image which has uniform intensity. Let $\mathbf{I}_{const} = [a \ldots a]^T$ be a column vector representing the uniform background. The correlation of a model with this uniform background vector yields the following result:

$$C = \frac{\mathbf{M}^T \mathbf{I}_{const}}{||\mathbf{M}||\ ||\mathbf{I}_{const}||} \ .$$

Substituting the value of $\mathbf{I}_{const}$ we get

$$C = \frac{\sum_{i=1}^{M_h M_w} m_i}{||\mathbf{M}|| \sqrt{M_h M_w}} \qquad (9)$$

where $m_i$ is the $i$th element of $\mathbf{M}$. We see that we get a correlation value that depends only on the model. We also see that the choice of origin affects the value of the correlation score. This is easily illustrated by remembering that the normalized

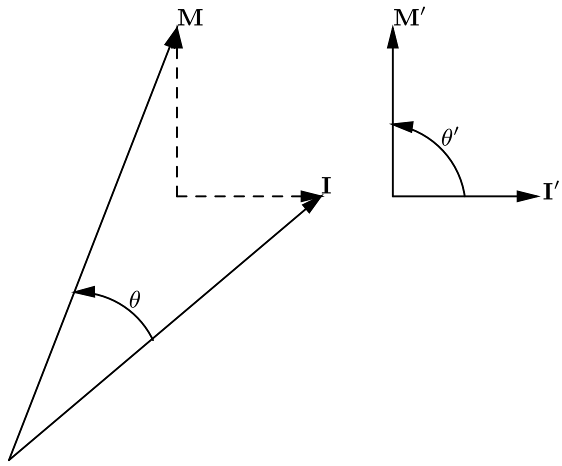


**Fig. 5** In this figure we see the effect of the choice of origin on the correlation score computed for the two vectors. On the left we see two vectors which could easily result from a positive-only imaging system, and the angle between them. On the right we see a much larger angle achieved by choosing a different origin for the vector coordinates. In general, for any two distinct vectors it is possible to choose an origin which makes the angle between them any value, including 90 and 180 degrees.

correlation score is just the cosine of the angle between the two vectors, i.e. $C = \cos\theta$ where $\theta$ is the angle between $\mathbf{M}$ and **I**.

In Figure 5 we see a graphic depiction of the effect of choice of the origin on the correlation score. On the left we see a pair of vectors, $\mathbf{M}$ and **I**, which could be a typical pair of image vectors. The angle between the two vectors is $\theta$, which is directly related to the correlation score (smaller angles correspond to higher correlation scores, and *vice versa*). When all the vector components are positive, then the resulting image vectors are limited to a subset of the image space. In the 2-D case shown here (think of the image vectors as having two pixels), the vectors are limited to one quadrant of the vector space. In the 3-D case (think of the image vectors as having three pixels), the vectors are limited to one octant of the vector space. In general, the image vector will be confined to $\frac{1}{2^N}$ of the space, where $N$ is the total number of pixels in the image. Since the models we are searching for will routinely have hundreds and even thousands of pixels, we see that the net result of having only positive components in the vectors is that correlation scores will tend to be high in most cases. On the right of Figure 5, the same two vectors are depicted, but a new origin is being used. In this case the vectors are represented by $\mathbf{M}'$ and $\mathbf{I}'$, and the angle between them is $\theta'$. In this case the origin has been chosen to make $\theta' = 90°$. In general, we can choose the origin to make the correlation score anything we want (we can only make $C = 1$ in the limiting case where the origin tends to infinity).

Given an infinite number of choices for a new origin, which one should we choose? One reasonable choice would be to choose an origin such that correlation of the model with a uniform background leads to a score of $0$. Examining Eq. 9, we see that subtracting the mean of the model vector components from the model will cause

$$\sum_{i=1}^{M_w M_h} m_i' = 0 \ .$$

Since a correlation score of $+1$ indicates a perfect match, and a score of $-1$ indicates a perfect mismatch, then a score of $0$ for comparison with a featureless background seems reasonable. This method of subtracting the mean from the model has been very successful in practice. It should also be noted that subtracting the mean from the model is the equivalent of removing any D.C. component from the model image's energy—thus only the energy related to model features is left.

A final issue to consider involves the effect of subtracting the model's mean from the image region being correlated with the model. While it seems reasonable in practice to treat the image region in an identical fashion to the model, there are some practical problems. If the mean is subtracted before the normalization is applied, then raw intensity of the model can affect the matching process. Since one of the reasons we use NGC is for its robustness against changes in image intensity, this is undesirable. In an image captured with pixel values in the range $0 \ldots 255$, pure multiplicative changes about the origin ($0$) are equivalent to a translation and a multiplication when any other origin is chosen. It was observed in practice that subtracting the same mean from both the model and the image region being compared made the entire process very sensitive to changes in lighting. As a result, it is proposed that the mean of the image region be subtracted instead. In this case we are no longer doing pure NGC (since each vector has a different value subtracted from it), but it works far better in practice. Again, one can think of this as having removed the D.C. component from the image region.

### *3.3 Tuning the Pyramid*

Up until now the only mention made of $K$ is that it is limited by the size of the model. In many cases the details in the model may degrade too quickly for this limit to be realistic. Take, for example, a model which consists of a checkerboard pattern, with alternating pixels black and white. In this case even a 2-level pyramid is too much, because the second level of the model pyramid will be a uniform (featureless) grey region which will be useless for correlation.

Instead, the depth of the pyramid must be chosen according to the characteristics of the model itself. One method of doing this is to build the model pyramid one level at a time, and as each new level is added estimate the worst-case correlation score of the model with itself at that level.

By *tuning the pyramid* we refer to the problem of deciding how many levels to choose for a pyramid representation of a given model. Note that this concept is similar to the idea of finding an optimal template for matching, as described in [12], although in our case we are searching for an optimal representation based on a single exemplar, as opposed to combining multiple exemplar images into a template. The more levels the pyramid has, the greater the savings in computation, but building the pyramid with too many levels may render the model unrecognizable to the NGC algorithm running at the top of the pyramid. The following discussion on the effects of pyramid sampling gives a possible solution to the problem of tuning the pyramid.

*3.3.1 Issues Surrounding Sampling of the Pyramid* Usually a model is chosen as a sub-image in a larger image. It is possible that we will then look for other instances of that model in the same image, or we may wish to remember the model and try and find it again later.

Consider, for example, that we have a model of size $50 \times 50$ located at $(96, 96)$ in the image. The model pyramid will have 4 levels of size $50 \times 50$, $25 \times 25$, $12 \times 12$ and $6 \times 6$. If we look at the top-level of the model we will find an exact replica of it in the top-level of the image pyramid (save integer division truncation errors), since the location of the model is on an integral 8-pixel boundary, and our

4 level pyramid has a top-level where each pixel is represented by $8 \times 8 = 64$ pixels from the bottom-level. This guarantees that the same information is averaged and combined in the exact same way while building both the image and model pyramids. But what would happen if the model had been at $(97, 97)$? Then the top-level representation of the target is not the same in the image pyramid as in the model pyramid. Since at $(96, 96)$ the top-level instance will have a score of $1$, the score when the model is at $(97, 97)$ will generally be worse. For a two-level pyramid we require the model to be on an even pixel boundary in order for the image and model pyramid to match at the top. Therefore, for a randomly placed model there is one chance in four that it will land perfectly. For a three-level pyramid, the model must land on an even boundary of 4 pixels, giving one chance in sixteen of perfect alignment. There is one chance in 64 for perfect alignment in a 4-level pyramid.

It should be noted that perfect alignment is not required in order to be able to find the target at the top level of the pyramid. How well an imperfectly aligned model will match at the top of the pyramid is dependent on the features of the model.

*3.3.2 Tuning the Pyramid using Worst-Case Analysis* As discussed earlier, the representation of a target at the top of the pyramid may be better or worse depending on its location in the image. This suggests a possible method for tuning the pyramid.

The first step is to set an upper limit on the number of levels in the pyramid. Obviously correlation is meaningless with only one pixel at the top level of the pyramid, so we can choose a minimum size for the model at the top-level. For the current implementation of the search tool this minimum size has been chosen to be $4 \times 4$. This means that the maximum number of levels in the pyramid will be chosen so that the model has a minimum dimension between $4$ and $7$ (a minimum dimension of $8$ could be reduced to $4$ by adding another level to the pyramid). Depending on the features of the model it may be possible to successfully search at this maximum pyramid depth.

The second step is to consider the worst-case score of the model at different pyramid depths. The worst-case will be be due to the effects of pyramid sampling as discussed in Section 3.3.1. In order to determine the worst-case score of a model in a $K$-level pyramid, we build the model pyramid to $K$ levels, and then build a test pyramid based on the model but with offsets $(x, y)$ where both $x$ and $y$ are in the range $0 \ldots 2^{k-1} - 1$. Therefore we end up considering $2^{2(k-1)}$ different offsets at each pyramid level $k$. Of course, the offset $(0, 0)$ is expected to have a score of $1$.

It is important to note that this worst-case analysis is only an estimate of the worst score of the model at the top of the pyramid, since in a real search situation that score will depend on image content outside the target for which we have no *a priori* knowledge. As we consider different offsets, the size of the test pyramid (really just a shifted version of the model) can be as much as one-pixel smaller than the model in each level. If we consider the most extreme case, we compare a $4 \times 4$ model to a $3 \times 3$ test-image. In this case our estimate involves comparing $56.25\%$ of the model with a shifted version of itself.

The third step is to perform this worst-case analysis for pyramids from level 2 up to and including the maximum possible number of levels, and choosing the maximum pyramid depth that still yields an acceptable worst-case score.

A number of pathological targets can be imagined in order to test this scheme. Consider black & white checkerboard patterns where each cell of 2 white and 2 black squares takes on the following dimensions: $2 \times 2$, $4 \times 4$, $8 \times 8$ and $16 \times 16$. The first pattern can only be searched with a 1-level pyramid, since the $2 \times 2$ receptive field used to go to the next level will blur the checks into a featureless pattern of grey. The second pattern could be searched with a 2-level pyramid if we were confident that the target would always align perfectly on a 2-pixel boundary. However, since this is not guaranteed, we will likely end up with a featureless grey again (corresponding to an offset of $(1, 1)$), so we must restrict ourselves to a 1-level pyramid. The next two patterns (for similar reasons) may be searched reliably with a 2-level pyramid, but no more.

To recap the worst-case analysis algorithm, we perform the following steps:

1. Based on the size of the model in the original image, determine the maximum depth (number of levels) of the pyramid that will make the top-level representation of the model larger than a pre-set minimum size (in our case $4 \times 4$ pixels). Call this depth $K_{max}$.
2. Build the model pyramid to this depth.
3. For each pyramid of depth $k$ in the range of $2 \ldots K_{max}$ perform a worst-case analysis of the test-image representation of the model at level $k$. This is done by building a test-image pyramid based on the original model, but offset by

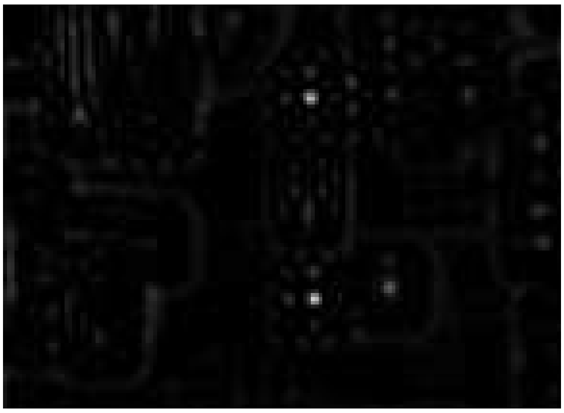

**Fig. 6** The correlation surface from the top level of the pyramid is shown. Two strong peaks, representing the location of the two instances of the model, are evident. These peaks provide coarse location estimates, which are refined as the algorithm descends through the pyramid.

$(x, y)$ where each of $x$ and $y$ takes on values in the range $0 \ldots 2^{K-1} - 1$. For each image, compute the correlation score between the $k$th level representation of the image and the model.

4. Choose the number of levels in the pyramid to be the largest value of $k$ for which the worst-case correlation score between model and test-image is above some pre-set threshold (currently we are using 0.1 for this threshold).

Intuitively this method is quite appealing, in that it mimics the actual search process when deciding how to tune the pyramid. Unfortunately, it may well be that always catering to the worst-case is unduly pessimistic. Variations on the method, in which the average or median of returned scores is used instead of just the worst-case itself, may prove useful.

The worst-case score found at the top-level of the model pyramid can be used to determine what threshold to use in accepting candidates at the top-level correlation. If, for example, the worst-case score is 0.7, and the correlation accept threshold entered by the user is 0.8, then the threshold for accepting candidates at the top-level could be set to $0.56 = 0.7 \times 0.8$. In this way candidates that are imperfect matches in the original image, and whose scores degrade in coarser pyramid levels, can still be found by the algorithm.

## 4 Implementation, Experiments & Results

The algorithm has been implemented in C++, and compiled on a Windows-based PC using Visual C++ V6.0. The core algorithms are not Windows specific and can be (and have been) re-compiled on other platforms, including Linux. No special effort has been made to optimize the run-time efficiency of the code. The results that follow are from an AMD Athlon Thunderbird 750 MHz system with 256 MB of RAM. In all cases the accept threshold is set to 0.75, representing a correlation score of $0.866 = \sqrt{0.75}$. Except where otherwise noted, the algorithm has been given the expected number of targets in advance. Results are given for search time *vs.* number and size of targets and false positive/negative results are also given. Finally, the algorithm is tested for sensitivity to slight variations in scale and rotation of the targets. Results are also shown for real-world images where the target undergoes mild perspective distortion. Finally, the performance of the algorithm with respect to sub-pixel localization is presented.

### 4.1 Comparison with Full Correlation

To demonstrate the speedup of our method over full correlation (no pyramid structure or gradient search), the two were compared for a typical image search. The search shown in Figure 16(a) was conducted on the full-sized image, $2272 \times 1704$pixels , using a target $260 \times 96$ pixels in size. Our method required 0.547 seconds[2] The same search performed using full correlation yielded identical results, but took 450.922 seconds to complete. Both the search and target images were resized by 50%, and the experiment repeated. This time our method took 0.312 seconds, while full correlation required 29.375 seconds. By way of confirmation, note that $450.922/16 \approx 28$, suggesting that the full correlation result scales roughly according to the inverse of the product of the search and target pixel counts, as expected. This simple experiment demonstrates the potential speedup using our technique.

### 4.2 Top-Level Correlation Scores

As an example of how candidate scores can degrade in higher (coarser) levels of the pyramid, Table 1 shows the squared-correlation scores at the lowest and highest pyramid levels for the target instances shown in Figure 2. Instance 1, which also serves as the model, has perfect scores at both levels as we might suspect. However, instance 2 has a score of 0.950 at the lowest level (the original search image), but a poorer score of 0.796 two levels higher in the pyramid.

[2] This test was performed using a VMware virtual machine running Windows XP, on a host machine running Ubuntu Linux on a 2.16 GHz Centrino Duo processor.

| **Instance** | **Location** | **Score (level 0)** | **Score (level 2)** |
|---|---|---|---|
| 1<br>(model) | (322,304) | 1.000 | 1.000 |
| 2 | (318, 95) | 0.950 | 0.796 |

**Table 1** Squared Correlation Scores for Model in Figure 2

### *4.3 Search Time* vs. *Number of Target Instances*

Results are shown in Figure 7 for the effect of number of target instances on the search time. In the lower trace we see that as the number of instances increases, the search time increases in a roughly linear fashion. This is to be expected. The search time can be thought of as the overhead of building the pyramid representation of the search image, plus the time to evaluate individual candidates. If the algorithm has already found the requested number of target instances, it can terminate early. If it does not have an upper bound, then it will continue to evaluate candidates until no more suitable candidates are found in the top-level correlation. This may prolong the search if the image contains distractor patterns that are sufficiently similar to the target. This extra time may be reduced by setting a higher accept threshold, which in turn causes less candidates to be considered at the top-level correlation. The upper trace in the figure is an example of roughly constant search time in the case of not knowing how many instances to expect. In this case, random distractor blobs were used to test the algorithm's ability to find the correct target. When distractors are not present, the search time in both cases is very similar.

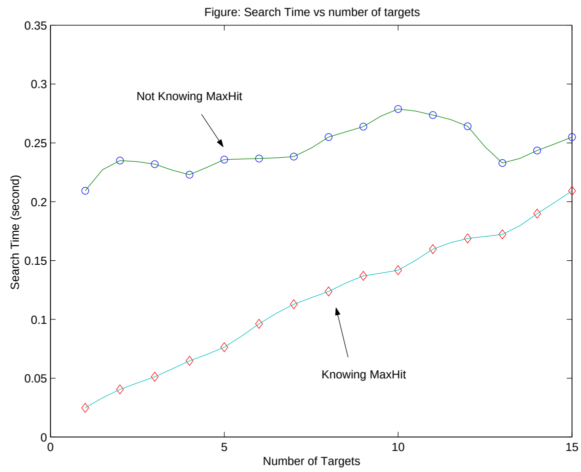


**Fig. 7** This figure shows the increase in search time as more target instances are found. In the upper trace the algorithm does not know the number of targets to expect in advance, and has to consider distractor blobs in the image. In the lower trace it knows the expected number of targets, illustrating the advantage of giving the algorithm an upper bound on the expected number of targets.

It should be noted that in the case where multiple targets are to be searched for in the same image, the overhead of constructing the image pyramid will only be required once, leading to more efficient searches.

### *4.4 Search Time* vs. *Size of Model*

Using NGC in a non-pyramid framework we would expect search times to increase as the size of the model increased. As the model size increases, we reach a point where another level may be added to the model pyramid (depending on the results of the worst-case analysis), resulting in a *smaller* model at the top of the pyramid, as well as a smaller search image at the top of the pyramid. There is extra overhead to build one more level in the search pyramid, but this gets smaller for each level of the pyramid by a factor of 4, and the savings in correlation computations more than offsets this. It should also be noted that rectangular models use the minimum dimension to limit pyramid size, so this further complicates the relation between size and search time.

In Figure 8 we see the results of varying model size on search times with the number of target instances held fixed, and the size of the image being searched held fixed. The results shown are from a set of real images captured using a camera at varying distances from the target and distractors. In the graph we see that search times gradually increase as the target is increased in size to 50 pixels, then they suddenly decrease, only to incease to a new maximum at 70 pixels, and finally another increase to a new maximum at greater than 100 pixels. The point at which new pyramid levels are built is further controlled by the worst-case analysis, so changes may not occur exactly at sizes that are an even power of 2. The line joining the data is a smooth interpolation. For small model sizes we may not see the same pattern of increases and decreases as the algorithm places a hard-limit on the smallest allowed model at the top of the model pyramid, thus preventing the pyramid from attaining its full depth in some cases.

It is instructive to develop a simple model explaining the search-time as a function of model size. Assume we have a model of size $n \times n$ in an image of size $I_w \times I_h$. The total search time (up to the end of the top level correlation) can be written as $T = T_s + T_p$ where

$$T_p = C I_w I_h \left( 1 + \frac{1}{2^2} + \frac{1}{2^4} + \cdots + \frac{1}{2^{2(m-1)}} \right)$$

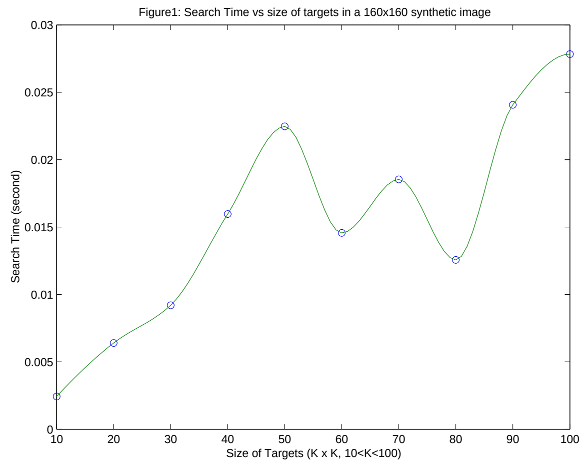


**Fig. 8** This plot shows search time as the model size is increased. The peaks occur when the model size is smaller than the size which would incease the number of levels in the model pyramid. There is also an increase in subsequent peaks due to extra overhead required to build the search pyramid. The model used for this figure was a black-on-white cross.

is the time required to build the pyramid. Here, $C$ is a constant relating the search cost $T_s$ to that of building the pyramid, and $m = \lfloor \log_2 n \rfloor$ is the height of the model pyramid. We also write

$$T_s = \left\lfloor \frac{n}{2^m} \right\rfloor^2 \left\lfloor \frac{I_w}{2^m} \right\rfloor \left\lfloor \frac{I_h}{2^m} \right\rfloor .$$

Figure 9 shows the predicted ideal search time with $n = 10 \ldots 150$, $I_w = I_h = 300$. Note how the early peaks in $T_s$ are hidden by the cost of pyramid construction. This same effect is also evident in Figure 8.

### 4.5 Accuracy

Determining the accuracy of the search algorithm is subjective as it can be used to find instances of patterns that are very similar but not identical. Tests with an

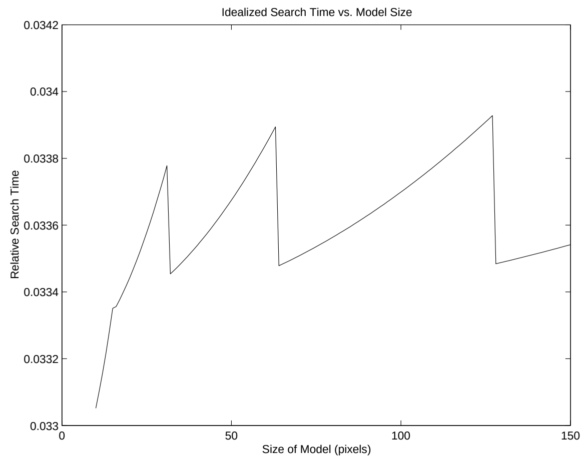


**Fig. 9** Idealized search times generated by search complexity model. Notice the similarity to Figure 8. As the relative cost of building the pyramid increases, early peaks in the plot are smoothed out.

accept threshold of 0.95 have yielded a false positive rate of less than $0.1\%$. As the threshold is lowered, the algorithm will match instances with increasing variability. In the extreme, one could imagine matching anything with an accept threshold of 0. Even an accept threshold of 0.75 may miss target instances which we would consider good, as is shown in Figure 10 (a). In this case, a change in the background surrounding the instance, plus different shading in the middle of the target, is enough to cause its rejection at this threshold level. The important thing to recognize here is that correlation scores do not always coincide with perceptual judgements. Occlusion and shading are also known to adversely affect correlation matching, and are not explicitly examined in this section.

False negative rates are affected not only by accept threshold, but also by the maximum target instance parameter if it is specified. Target instances may also be

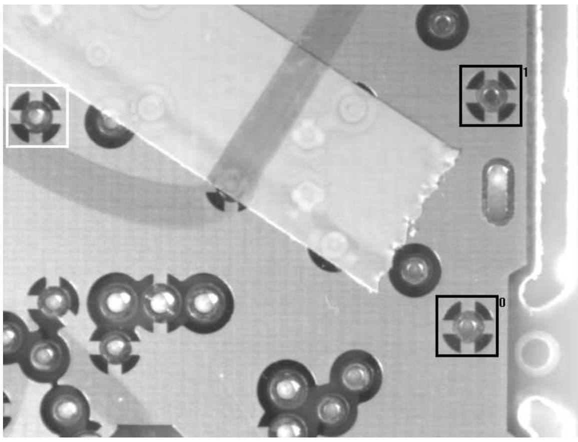

(a)

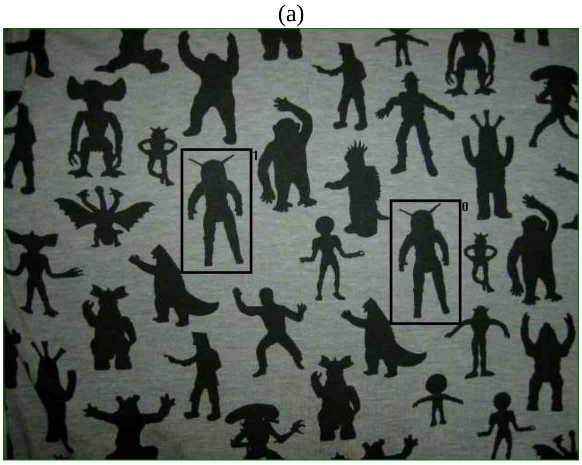

(b)

**Fig. 10** Two images in which searches have taken place. In (a) we have an example of a false negative (white box), but the missed target instance is noticeably different due to background shading. In (b) we have no false results despite relative similarity of all objects in terms of size and intensity levels.

rejected if they cross the borders of the image, as the current implementation only looks for instances wholly contained within the search image. In summary, almost all false results occur when the target instance is not identical, or close to identical, to the model.

### 4.6 Sensitivity to Small Scale and Orientation Changes

Even though normalized correlation is not designed to accomodate changes in scale and orientation, tests show that in some cases it may do quite well. In Figure 11 correlation scores are shown for small changes in scale and orientation of the target instance.

These results suggest mechanisms by which scale and orientation invariance might be built into the algorithm. In the case of scale, the pyramid would easily allow for searching over different scales separated by a factor of 2. If we create a number of re-scaled versions of the model to be searched at each pyramid level (in this case each about 1.2 times larger/smaller than the previous one), then the algorithm could be used to search over the range of $1/\sqrt{2}$ to $\sqrt{2}$. Anything larger or smaller could be searched in the next scale. A schedule for searching at the different pyramid levels can be devised, and the number of additional models required at each level can be determined via worst-case analysis. In the case of rotation, a method similar to that of [26] can be used to determine the number of additional target templates required to search for rotated versions of a target.

### 4.7 Subpixel Localization

In identifying an object in an image using NGC, it may be the case that the object as found will not align with the pixel grid in the same way as the model (or template)

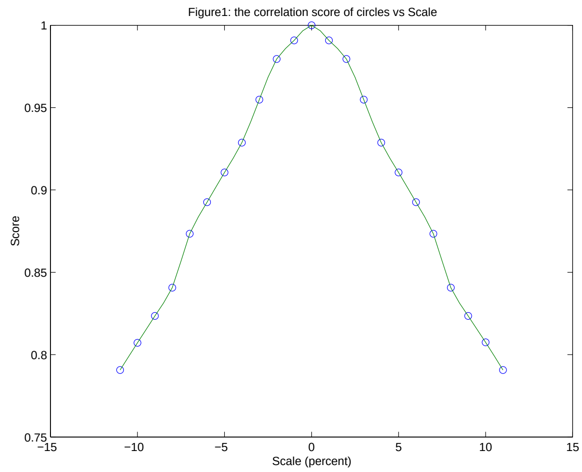


(a)

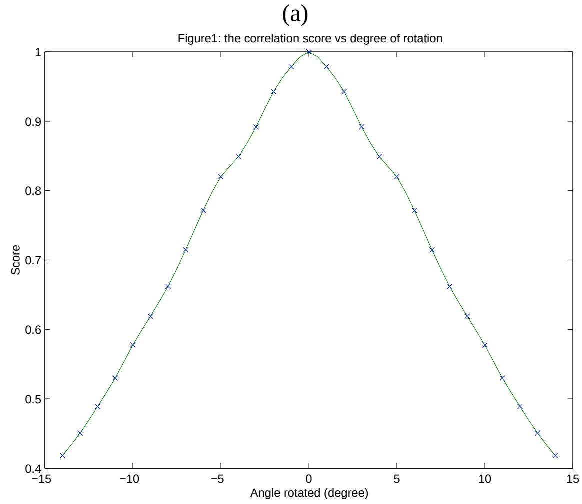


(b)

**Fig. 11** This figure shows the effect of slight changes in both (a) scale and (b) orientation on the correlation scores. Scale was varied by $\pm 10\%$ resulting in correlation scores from 0.8 to 1.0. The target used was a black ellipse on a white background. Orientation was varied by $\pm 14^\circ$ resulting in squared-correlation scores from 0.418 to 1.0. The target used was a black cross on a white background. The use of simple, high-contrast targets is intended to isolate the method's ability to recognize shapes.

did. In this event, our estimate for the location of the object is expected to lie *between* pixels. Since NGC only allows us to compute the correlation at integral pixel locations, some method of determining the sub-pixel location is needed. One such method is interpolation using a *bi-quadratic* surface as described in [20]. In this section we give performance results for this method.

Two sets of tests were done. The first set involves a series of 10 images produced by synthetic means. Software was devised to simulate a target moving in the horizontal direction at 0.1 pixels/frame. The main advantage to using synthetic images is that ground truth is known for the target location. However, the synthetic data ignore the possibility of effects introduced by imperfections in the imaging system.

The synthetic images were created by creating a target at a higher resolution than the original image, and then averaging over the required subset of pixels in order to determine the target's representation in the low-resolution image.

The second set of images involve a printed circuit board, with the board being shifted left by roughly $1/20$ of a pixel in each subsequent image using a camera mounted on a mechanical X-Y translation stage. No absolute orientation between the camera and the stage is sought—the important thing is that the base of the stage is stationary with respect to the scene, so the changes between images is solely related to the controlled movement of the camera. The method of fixing the camera to the stage rougly aligns the camera's horizontal and vertical directions to those used by the stage itself. There are 20 images in the sequence. This image sequence permits meaningful testing of the subpixel localization algorithm on real images.

In both sets of images, the model is defined in the first image, where its location (by definition) lies exactly on an integer pixel boundary. In each image sequence the target is assumed to shift by roughly equal amounts from one image to the next.[3] As a model is tracked, therefore, the subpixel estimate for its location should form a straight line with respect to the frame number.

For analysis of the images, four image regions were selected as models, and each region was searched in each image in order to obtain an estimate of its location using subpixel localization.

*4.7.1 Subpixel Localization—Synthetic Images* Figure 12 shows the results of subpixel estimation in the horizontal direction. The data has been shifted to show the movement in the range of $0$ to $1$.[4] The error in the estimates ranges from $0.0018$ pixels (when the target position is integral) to a maximum of $0.0886$ pixels. The mean error for the synthetic data is $0$ (when taken over a complete cycle of the error curve). The RMS (root mean squared) error is found to be $0.06$ pixels. Errors in the localization may be related to the fact that the interpolation scheme does not constrain the correlation to have a maximum of 1.0 for the estimated bi-quadratic surface. They may also be related to the interpolation used to generate the synthetic images.

---

[3] For the synthetic images this is known to be true, for the real images this was the intention, and will be true within limits on physical precision of the translation stage.

[4] In the original image, the horizontal location of the target starts at 318 pixels.

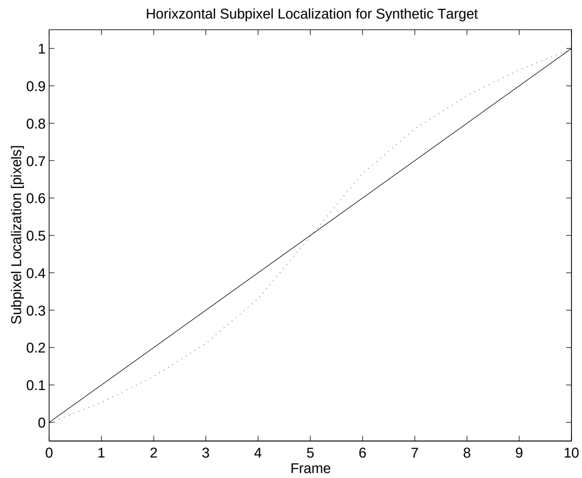


**Fig. 12** This image shows the localization in the horizontal direction of the moving target (black-and-white cross). The solid line indicates the ground truth position for the target, and the dotted values the subpixel localization estimates. The error is roughly symmetric about the half-way point between integral pixel values.

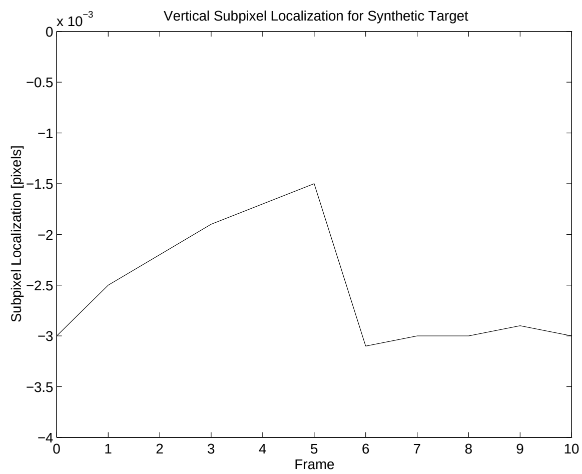


**Fig. 13** This image shows the localization in the vertical direction of the moving target. There was no target movement in this direction, so ideally the error should be zero. The sudden change in the error at frame 5 is likely due to the search algorithm switching its (pre-subpixel) best estimate for the target from one pixel to the next.

Figure 13 shows the vertical error. Since the target was not moving vertically, we expect this error to be roughly constant, and ideally $0$. The mean error was $-0.0025$ pixels, and the RMS error was $0.0026$ pixels. We see a sharp change in the error around frame 5. To understand this, recall that the subpixel localization algorithm starts from $9$ correlation values centred on the best integral estimate of the target position. At frame 5 we are half-way between pixels, and we should expect the best integral estimate to switch from one pixel to the next at this point.

*4.7.2 Subpixel Localization—Structured Images* The data derived from the four image regions tracked through a real image sequence, of a printed circuit board, was analyzed in an attempt to gauge the performance of the subpixel localization algorithm. First, since it was assumed that all movement in the image sequence was purely in the horizontal direction, any changes in the vertical ordinate of the estimates should represent noise. In Figure 14 we see a plot of the $y$-ordinates from the four data sets. Each data set has been adjusted to start at 0 so that they could be plotted together. The mean error, $\bar{y}$ is calculated as

$$\bar{y} = \frac{1}{N} \sum_{i=1}^{N} y_i$$

where $y_i$ are the adjusted $y$ data. The value obtained is 0.003 pixels. Since each target is defined in the first image in the sequence, we expect the error to have zero average over the image sequence, assuming the translation stage is properly aligned with the camera. The root-mean-square error, defined as

$$\sigma_y = \sqrt{\frac{1}{N} \sum_{i=1}^{N} (y_i - \bar{y})^2}$$

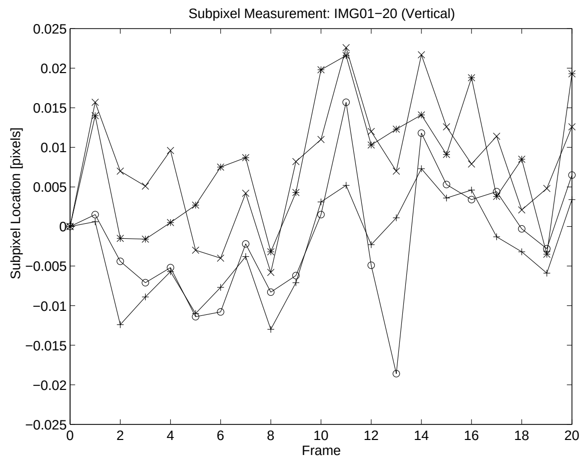


**Fig. 14** This figure shows the vertical ordinates of the subpixel localization estimates over the entire image sequence. The estimate shown for Frame 0 is that obtained with subpixel localization turned off. Each data set has been adjusted so that the first element is zero. Data sets 1–4 are represented by *, +, X and o, respectively.

was measured to be 0.009 pixels. As expected from looking at Figure 14, this error is quite small.

Unlike the vertical ordinates, the horizontal ($x$) ordinate estimates are expected to change. Since the image moves approximately one pixel to the left over 20 frames, we would expect a change of about $-0.05$ pixels/frame. As seen from the plot in Figure 15, the slope of these lines is indeed negative, and a quick estimate shows it to be approximately the right size. In order to get a more accurate measure of the error, a linear least-squares regression was performed on the data.

Figure 15 shows the best-fit line from the regression done assuming the line had zero intercept. The line has a slope of $-0.0356$ pixels/frame. The mean error in the data with respect to the regression line is $-0.0034$ pixels, and the RMS error is $0.09$ pixels.

Another meaningful test is to pick out multiple regions in an image as targets, and then search for them in the same image. In this case the exact target location is known, and it is known to be an exact integral value. The subpixel location estimates will not return exactly integral values and are expected to be in error—the question is “how much?”. In a set of data collected using this approach (15 regions), the horizontal location error was found to have a mean error of $0.0676$ pixels and an RMS error of $0.1264$ pixels in the horizontal direction. The corresponding values for the vertical direction are $0.0094$ and $0.0305$ pixels, respectively. It must be mentioned that several of the targets were structure deficient, *i.e.* they were composed of lines almost exclusively in one direction, in this case horizontal, leading to some large error values in the horizontal estimate. The mean and RMS error values would doubtlessly be lower if these samples were omitted.

### *4.8 Results From Unstructured Scenes*

In this section, real-life examples of searching for targets are presented. In Figure 16 two examples are shown of images acquired at a car dealership. In Figure 16(a) the technique is applied to find matches for the front end of the middle car. Due to perspective distortion, the front-end details of the cars to both the right and left of centre are noticeably different from those of the centre car. While the squared correlation scores drop to 7.0 and 7.5 for the immediate neighbours, and

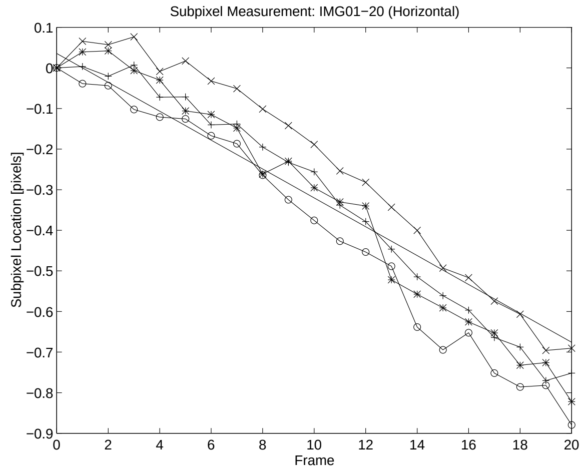


**Fig. 15** This figure is the same as Figure 14, except that here the horizontal ordinate of the subpixel localization estimate has been plotted. Over the 20 frames in the sequence, we see that the image shifts to the left by about 0.9 pixels. It shows the best-fit line (least-squares regression) fitting the subpixel location estimates.

5.6 and 5.1 ($C = .714$) for the outside cars, this is still well above the threshold where false negatives appear, namely $C^2 = 0.32$.

A further test was carried out using the car lot image. A sequence of images was created by taking the original target, and searching for it in the car image corrupted by adding independent Gaussian noise with values of $\sigma$ ranging from $1$ to $10$. The original target instance was correctly identified in each case, although the correlation score dropped from 1.0 for the noise-free image, to $C = 0.988$ for $\sigma = 1$ and $C = 0.9822$ for $\sigma = 10$. Since noise in modern CCD cameras is typically less than $\sigma = 10$, additive Gaussian noise is not a large problem for the algorithm.

In Figure 17 we show results for images similar to those used in [4]. The target (Figure 17(b)) was obtained by scanning Waldo's face from the instruction page at the front of "Where's Waldo? The Wonder Book" [8]. This image was rescaled by eye to approximately match the size it appears elsewhere in the book using the GIMP (GNU Image Manipulation Program). The target image was $21 \times 40$ pixels in size. The search was performed on a grey-scale version of the images, and was successful, as shown in the subset of the search region reproduced in Figure 17(a). The squared correlation score was $0.37$ ($C = 0.608$), which is good considering the slight changes in the details of Waldo's face and the dot-screening process used to print the book (we do not expect the dots on the target to align exactly with those in the recovered instance). Finding Waldo without colour is helpful, since in at least one Waldo image all other characters are dressed just like Waldo, meaning a method such as [4] that only uses colour information will be confounded. However, if colour information is helpful, our method can use colour correlation instead of grey-scale to take advantage of colour as well as image structure.

### *4.9 Timing Comparison with Feature Detectors*

In order to better describe the performance of our method, this section provides some timing comparisons with a number of current feature detectors, including SIFT and some affine-invariant techniques.

In Table 2 we see a timing comparison of a number of feature detectors. The first two entries in the table give different reports of SIFT detectors, and both show times of 0.3 seconds for small images [34] and medium size images [19], even

(a)

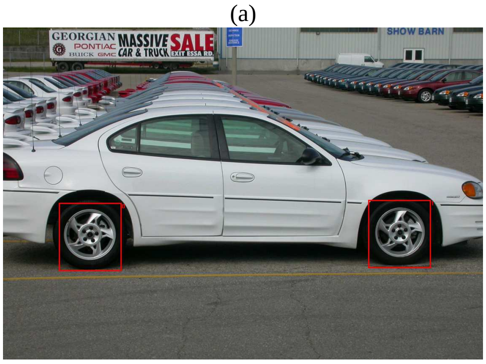


(b)

**Fig. 16** Two examples from unstructured images are shown. In (a) the target was chosen from the centre car, and squared correlation scores range from 0.51 for the car on the extreme left to 1.0 for the centre car as expected. This example shows performance in the presence of a moderate amount of perspective distortion. In (b) the target was chosen from the left wheel, and the right wheel is recovered, despite the presence of some rotation, as well as differences in the brake and pavement details.

though the latter is using a much faster processor than the first (or than the processors used in this paper). The next four entries are found in [25], which contains a comparison of a number of affine-invariant feature detectors. Both the Harris-Affine and the Hessian-Affine attempt to localize the feature, and compute an ellipsoidal region describing its scale and orientation (as opposed to Mikolajczyk & Schmid's affine-invariant detector, which iteratively warps the image around the feature point to create a circular region). IBR (intensity extrema-based region detector) explores regions around intensity extrema, using an affine-invariant func-

(a)

(b)

**Fig. 17** In (a) we see an example of “Where’s Waldo?”. Our algorithm easily finds Waldo in the lower-left corner. The target, shown enlarged in (b), was taken from the instructions at the front of “Where’s Waldo? The Wonder Book” [8], while the search region (a subset of which is shown in (a)), was scanned from later in the book (“The Corridors of Time” page). The match score was $C^2 = 0.37$, but given the slight differences in Waldo’s appearance and the dot-screening process used to print the book, this is quite good for a correlation-based search technique. [Permission to reproduce these images courtesy Mike Gornall, Egerton, Kent, England.]

| Algorithm | Time | Image Size | Hardware | Reference |
|---|---|---|---|---|
| SIFT | 0.3–0.4 S | $340 \times 240$ | Pentium III 700 MHz | [34] |
| SIFT | 0.3 S | $640 \times 314$ | Pentium IV 2 GHz | [19] |
| Harris-Affine | 1.43 S | $800 \times 640$ | Pentium IV 2 GHz | [25] |
| Hessian-Affine | 2.73 S | | | |
| MSER | 0.66 S | | | |
| IBR | 10.82 S | | | |

**Table 2** This chart shows a comparison of the running time of several popular feature detection algorithms.

tion of intensity evaluated along radial lines, and the loci of the extremums of this function are approximated by an ellipse, whose scale and orientation define the feature region. MSER (maximally-stable extremal regions) identifies regions based on their intensity with respect to a threshold, and finds regions that are stable over a number of threshold levels [1]. Note that feature computation times for the non-SIFT features does not include grouping or matching against known objects. We see that even SIFT, although it is closest in terms of computation time to our method, is still somewhat slower that our technique.

The MSER detector is the only other detector whose speed comes close to SIFT, albeit for larger images and running on a faster processor than used in this paper. While these detectors have similarity/affine invariance that our method does not provide, our method typically runs faster, and may prove useful in situations where only translation invariance is required. One such example is automated visual inspection tasks where the part under inspection has a known orientation and distance with respect to the camera.

## 5 Discussion

In Section 4 we see that our method has good performance in finding targets even in the presence of small amounts of rotation and scale change.

The algorithm is also very fast even on modest hardware, making it attractive for machine vision applications in industry. Only two other methods, those of Lowe [18] and Schiele & Pentland [32] cite similar speeds. Since the latter system is designed for detection, and not localization, we will not consider it further. In comparing our algorithm to that of [18], we note that it is more complex to implement than our algorithm, and that its method of finding features through analysis of feature stability across scale makes it less suitable for searching for small targets such as that shown in Figure 17(b). Further, we expect our method to better detect subtle differences in target instances as it does a pixel-by-pixel comparison. As mentioned in Section 2, Lowe's algorithm uses features that may fail to match under global illumination changes, causing the search to fail. While it may be possible to correct this using features such as those in [3], this would incur considerable computational expense and hinder the speed of the algorithm. Our algorithm, being based on NGC, is robust over a wide range of global illumination changes. In defense of SIFT, it has rotation and scale invariance while our method does not. This is a great advantage. Finally, our algorithm is applicable to techniques such as those cited by [37, 26], since these techniques perform matching by correlating candidate images against a set of templates determined by PCA. It is possible that a combination of our method with that of [26] would allow efficient search for rotated targets. Further, searching for slightly re-scaled versions of the target across pyramid levels (as described in Section 4.6) would allow our method to find targets across a range of scales.

The speed of the search is largely dependant on the number of levels in the target pyramid. In the case of the checkerboard pattern where each square is one pixel, we expect performance to be very slow since only one level exists in the pyramid, and the algorithm is reduced to that of ordinary NGC. Nonetheless, it will still work. In practice such degenerate target patterns are the exception and not the rule, and the system typically works with a 3- or 4-level target pyramid, resulting in substantially faster operation.

The choice of the accept threshold will have a strong effect on the results. As this threshold is reduced we would expect to find a larger number of false positives. Of course, it is somewhat subjective as to what constitutes a match in the first place, and this will vary depending on the task for which the search is used. It must be remembered that lowering the accept threshold also leads to a larger number of candidate matches at the top level of the pyramid, and this in turn will generally lengthen the search time.

## 6 Conclusion

This paper describes a novel approach to pattern matching based on normalized correlation matching in a pyramid image representation. Three main contributions are made: (1) incorporation of NGC search into a multi-scale image representation, (2) use of an estimate of the correlation gradient to perform steepest descent search at each level of the pyramid, and (3) a method for choosing the appropriate pyramid depth of the model using a worst-case analysis. The result is a fast and robust method for localising target instances within images. Further, since it is based on correlation search, the technique is simple and easily combined with PCA techniques for target matching.

The algorithm is limited in that it does not attempt to deal with variable size or orientation of target instances, although it is shown to be robust to small variations in either parameter. The level of robustness is dependent on the actual pattern to be searched for, but this can be included in the worst-case analysis. The technique is also sensitive to image warping due to out-of-plane rotations, although again a small amount can be tolerated. A procedure for allowing size-invariant searches is outlined. Future work includes further investigation of size, and even orientation, invariance in the search framework.

Possible applications for this algorithm include machine inspection of printed circuit boards, finding parts in an industrial setting, and identifying trademarks and copyright material on the Internet. In this latter vein the authors have built a search engine that follows HTML links, download images and searches them, and records the URLs of any matches found. Through judicious choice of the accept threshold, unauthorized modifications to trademarks were also found.

**Aknowledgements**

The authors would like to thank Fernando Nuflo and Fang Liu for their contributions to the testing of the algorithm.

**References**

1. A. Baumberg. Reliable feature matching across widely separated views. In *IEEE Conference on Computer Vision & Pattern Recognition*, pages 774–781, 2000.
2. P. Burt. Attention mechanisms for vision in a dynamic world. In *Proceedings of the International Conference on Pattern Recognition*, pages 977–987, 1988.
3. Gustavo Carneiro and Allan D. Jepson. Multi-scale phase-based local features. In *Proceedings of the IEEE Computer Society Conference on Computer Vision and Pattern Recognition*, volume 1, pages 736–743, Madison, WI, June 2003.
4. François Ennesser and Gérard Medioni. Finding Waldo, or focus of attention using local colour information. *IEEE Transactions on Pattern Analysis and Machine Intelligence*, 17(8):805–809, August 1995.
5. Rafael C. Gonzalez and Paul Wintz. *Digital Image Processing*. Addison-Wesley Publishing Company, Reading, Massachusetts, 2nd edition, 1987.
6. Ardeshir Goshtasby. Template matching in rotated images. *IEEE Transactions on Pattern Analysis and Machine Intelligence*, PAMI-7(3):338–344, May 1985.
7. Michael A. Greenspan. Geometric probing of dense range data. *IEEE Trans. Pattern Anal. Mach. Intell.*, 24(4):495–508, 2002.
8. Martin Handford. *Where's Waldo? The Wonder Book*. Candlewick Press, 1997.
9. Chris Harris and Mike Stephens. A combined corner and edge detector. In *Proceedings Fourth Alvey Vision Conference*, pages 147–151, Manchester, United Kingdom, 1988.

10. Berthold Klaus Paul Horn. *Robot vision*. The MIT Press, Cambridge, Massachusetts, 1986.

11. M. K. Hu. Visual pattern recognition by moment invariants. *IRE Trans. Information Theory*, IT-8:179–187, 1962.

12. Y. S. Huang, C. C. Chiang, J. W. Shieh, and Eric Grimson. Prototype optimization for nearest neighbour classification. *Pattern Recognition*, 35:1237–1245, 2002.

13. Anil K. Jain and Aditya Vailaya. Shape-based retrieval: A case study with trademark image databases. *Pattern Recognition*, 31(9):1369–1390, 1998.

14. Jean-Michel Jolion and Azriel Rosenfeld. *A pyramid framework for early vision*. Kluwer Academic Publishers, P.O. Box 17, 3300 AA Dordrecht, The Netherlands, 1994. ISBN: 0-7923-9402-X.

15. Yong-Sung Kim and Whoi-Yul Kim. Content-based trademark retrieval system using visually salient feature. In *1997 Conference on Computer Vision and Pattern Recognition*, pages 307–312, Peurto Rico, June 1997.

16. Arun D. Kulkarni. *Artificial Neural Networks for Image Understanding*. Van Nostrand Reinhold, New York, 1994. ISBN 0-442-00921-6; LofC QA76.87.K84 1993.

17. Tony Lindeberg. *Scale-space theory in computer vision*. Kluwer Academic Publishers, P.O. Box 17, 3300 AA Dordrecht, The Netherlands, 1994. ISBN: 0-7923-9418-6.

18. David G. Lowe. Object recognition from local scale-invariant features. In *Proceedings of the Seventh International Conference on Computer Vision*, pages 1150–1157, Kerkyra, Greece, 1999.

19. David G. Lowe. Distinctive image features from scale-invariant keypoints. *International Journal of Computer Vision*, 60:90–110, 2004.

20. W. James MacLean and John K. Tsotsos. Fast pattern recognition using gradient-descent search in an image pyramid. In *Proceedings of 15th Annual International Con-*

*ference on Pattern Recognition*, volume 2, pages 877–881, Barcelona, Spain, September 2000.

21. Krystian Mikolajczyk and Cordelia Schmid. Indexing based on scale invariant interest points. In *IEEE International Conference on Computer Vision*, pages 525–531, 2001.
22. Krystian Mikolajczyk and Cordelia Schmid. An affine invariant interest point detector. In *European Conference on Computer Vision*, volume 4, pages 128–142, 2002.
23. Krystian Mikolajczyk and Cordelia Schmid. Scale and affine invariant interest point detectors. *International Journal of Computer Vision*, 60(1):63–86, 2004.
24. Krystian Mikolajczyk and Cordelia Schmid. A performance evaluation of local descriptors. *IEEE Transactions on Pattern Analysis & Machine Intelligence*, 27(10):1615–1630, 2005.
25. Krystian Mikolajczyk, Tinne Tuytelaars, Cordelia Schmid, Andrew Zisserman, J. Matas, F. Schaffalitzky, T. Kadir, and L. Van Gool. A comparison of affine region detectors. *International Journal of Computer Vision*, 65(1/2):43–72, 2005.
26. Hiroshi Murase and Shree K. Nayar. Visual learning and recognition of 3-D objects from appearance. *International Journal of Computer Vision*, 14:5–24, 1995.
27. Chahab Nastar, Baback Moghaddam, and Alex Pentland. Flexible images: Matching and recognition using learned deformations. *Computer Vision & Image Understanding*, 65(2):179–191, 1997.
28. Alex Pentland, Rosalind W. Picard, and Stan Sclaroff. Photobook: Content based manipulation of image databases. *International Journal of Computer Vision*, 18(3):233–254, 1996.
29. William K. Pratt. *Digital Image Processing*. John Wiley & Sons, Inc., New York, 2nd edition, 1991.
30. H. K. Ramapriyan. A multilevel approach to sequential detection of pictorial features. *IEEE Trans. Computers*, 25(1):66–78, 1976.

31. Aparna Lakshmi Ratan, W. Eric L. Grimson, and William M. Wells. Object detection and localization by dynamic template warping. *International Journal of Computer Vision*, 36(2):131–147, 2000.
32. Bernt Schiele and Alex Pentland. Probabilistic object recognition and localization. In *Proceedings of the Seventh International Conference on Computer Vision*, pages 177–182, 1999.
33. Stan Sclaroff, Marco La Cascia, and Saratendu Sethi. Unifying textual and visual cues for content-based image retrieval on the world wide web. *Computer Vision & Image Understanding*, 75(1/2):86–98, 1999.
34. Stephen Se, David Lowe, and Jim Little. Mobile robot localization and mapping with uncertainty using scale-invariant visual landmarks. *International Journal of Robotics Research*, 21(8):735–758, August 2002.
35. Josef Sivic, Frederik Schaffalitzky, and Andrew Zisserman. Object level grouping for video shots. In *Proceedings of the European Conference on Computer Vision*, volume LNCS 3022, pages 85–98, 2004.
36. Chris Stauffer and Eric Grimson. Similarity templates for detection and recognition. In *IEEE Conference on Computer Vision & Pattern Recognition*, Kauai, Hawaii, 2001.
37. M. Turk and A. Pentland. Eigenfaces for recognition. *Journal of Cognitive Neuroscience*, 3:71–86, 1991.
38. G. van der Wal and P. Burt. A VLSI pyramid chip for multiresolution image analysis. *Int. Journal of Computer Vision*, 8:177–190, 1992.
39. Harry Wechsler and George Lee Zimmerman. 2-D invariant object recognition using distributed associative memory. *IEEE Transactions on Pattern Analysis and Machine Intelligence*, 10(6):811–821, November 1988.
40. Harry Wechsler and George Lee Zimmerman. Distributed associative memory (dam) for bin-picking. *IEEE Transactions on Pattern Analysis and Machine Intelligence*,

11(8):814–822, November 1989.

41. J. K. Wu, C. P. Lam, B. M. Mehtre, Y. J. Gao, and A. Desai Narasimhalu. Content-based retrieval for trademark registration. *Multimedia Tools & Applications*, 3(3):245–267, 1996.